



**Environmental
Science**
Nano

Reactive halogen radicals in saline water promote photochemically-assisted formation of manganese oxide nanosheets

Journal:	<i>Environmental Science: Nano</i>
Manuscript ID	EN-ART-04-2022-000410.R1
Article Type:	Paper

SCHOLARONE™
Manuscripts

Environmental significance

Reactive halogen radicals form from abundant halides in saline surface water and in the highly saline water from energy-water recovery systems. Here, we demonstrate an undiscovered manganese oxidation pathway by reactive halogen radicals. This is the first report of reactive halogen radicals oxidizing transition metal ions and forming oxidized solids under environmentally relevant pH. Bromide radicals in particular greatly increase the rate of abiotic manganese oxidation. These findings advance our understanding of abiotic Mn^{2+} oxidation and Mn oxide nanosheets formation mechanisms, especially in oceans, estuaries, and brine water systems, which will play a significant role in global biogeochemical and elemental redox cycling. Given the ever-increasing amounts of halide-containing efflux from desalination water treatment and subsurface energy recovery systems, halides and reactive halogen species are becoming even more important in the formation of redox active minerals *via* mechanisms similar to Mn oxidation. This study emphasizes the unforeseen impact of reactive halogen radicals and predicts their reactions with heavy metal ions other than manganese in environmental systems.

1
2
3 **Reactive halogen radicals in saline water promote photochemically-**
4 **assisted formation of manganese oxide nanosheets**
5
6
7
8
9

10
11
12 Zhenwei Gao, Charlie Skurie, and Young-Shin Jun*
13

14
15
16
17
18 *Department of Energy, Environmental and Chemical Engineering, Washington University in St.*
19 *Louis, St. Louis, Missouri 63130, United States*
20
21
22

23
24
25
26 Address: One Brookings Drive, Campus Box 1180
27

28
29 E-mail: ysjun@seas.wustl.edu
30

31
32 Phone: (314) 935-4539
33

34
35 Fax: (314) 696-1223
36

37 <http://encl.engineering.wustl.edu/>
38
39

40
41
42
43 ***Environmental Science: Nano***
44

45
46 Submitted: April 2022
47

48
49 Revised: July 2022
50

51 * To whom correspondence should be addressed
52
53
54
55
56
57
58
59
60

Abstract

Halide ions are naturally abundant in oceans and estuaries. Large amounts of highly saline efflux are also generated and discharged to surface water from desalination processes and from unconventional oil and gas recovery. These highly concentrated halides can generate reactive halogen radicals. However, the redox reactions of halogen radicals with heavy metals or transition metals have received little attention. Here, we report an undiscovered fast oxidation of manganese ions (Mn^{2+}) by reactive halogen radicals. Hydroxyl radicals ($\cdot\text{OH}$) are produced by nitrate photolysis. While $\cdot\text{OH}$ play a limited role in the direct oxidation of Mn^{2+} , they can react with halide ions to generate reactive halogen radicals to oxidize Mn^{2+} . More Mn^{2+} was oxidized by bromide (Br) radicals generated from 1 mM Br^- than by chloride (Cl) radicals generated from 500 mM Cl^- . In the presence of Br radicals, the abiotic oxidation rate of Mn^{2+} to Mn(IV)O_2 nanosheets is greatly promoted, showing a 62% increase in $\text{Mn}^{2+}(\text{aq})$ oxidation within 6 hr of reaction. This study advances our understanding of natural Mn^{2+} oxidation processes and highlights unexpected impacts of reactive halogen radicals on redox activities with heavy metals and corresponding nanoscale solid mineral formation in brine. This work suggests a new, environmentally-friendly, and facile pathway for synthesizing MnO_2 nanosheets.

1. Introduction

Interdependent energy-water engineering systems inherently produce large volumes of briny water. To meet rapidly growing clean water demands, desalination processes are increasingly used, consistently generating highly concentrated brine efflux (1.5–2 times as salty as seawater) that are directly released into adjacent lakes, rivers, and near shore seawater.^{1,2} In unconventional oil and gas recovery through hydraulic fracturing, large amounts of concentrated flowback brine (0.9–4.17 M Cl^- , and 9–20 mM Br^-) can accumulate in the surface impoundment before further treatment.³ As examples, Marcellus and Fayetteville hydraulic fracturing flowback fluids contain about 160 g/L (4.5 M) of Cl^- and 1.8 g/L (22.5 mM) of Br^- .⁴ The contaminated surface water from the effluent disposal sites in Pennsylvania contain about 60 g/L (1.7 M) of Cl^- and 40 mg/L (0.5 mM) of Br^- .⁴ These highly concentrated halides can be oxidized by the hydroxyl radicals ($\cdot\text{OH}$) and triplet state dissolved organic matter to form abundant reactive halogen radicals (e.g., X^\cdot , $\text{X}_2^{\cdot-}$, $\text{XY}^{\cdot-}$, where X, Y = Cl, Br, or I).⁵ In seawater, which usually contains about 0.54 M Cl^- and 0.8 mM Br^- , the concentrations of their corresponding halogen radicals, e.g., $\text{Br}_2^{\cdot-}$ and $\text{ClBr}^{\cdot-}$, can be 3–4 orders of magnitude higher than that of $\cdot\text{OH}$.^{5,6}

Studies thus far have focused on the effects of reactive halogen radicals on the degradation and transformation of organic pollutants, such as microcystins in estuarine water,⁷ and various pharmaceuticals and personal care products (PPCPs) in water treatment processes⁸. In particular, compared to fresh water, seawater increased the photodegradation kinetics of domoic acid (a cis–trans diene) because the generated reactive halogen radicals selectively targeted dienes.⁶ In addition, reactive halogen radicals can participate in natural oxidative reactions of mercury (Hg) in the atmosphere. A study conducted in Alaska reported that atmospheric elemental Hg was rapidly converted to reactive gaseous oxidized Hg species by reactive halogen radicals.⁹ However,

1
2
3 the roles of reactive halogen radicals in inorganic aqueous systems, such as redox reactions with
4 heavy metal and transition metal ions, remain largely unknown.
5
6
7

8 Manganese (Mn) oxidation by reactive halogen radicals under the environmental relevant
9 conditions and the roles of reactive halogen radicals in the formation of Mn oxide minerals have
10 never been reported. Mn oxide solids are excellent scavengers of redox-active species and heavy
11 metals in nature, and they play significant roles in geochemical element redox cycling, carbon
12 mineralization, and biological metabolisms.¹⁰⁻¹² In nature, Mn oxide solids are known to be formed
13 by oxidation of $\text{Mn}^{2+}(\text{aq})$. In such processes, hitherto, $\text{O}_2^{\bullet-}$ has been considered as the most
14 effective radical accomplishing Mn oxidation in both biotic and abiotic systems.¹³⁻¹⁷ However, Mn
15 oxidation by reactive halogen radicals in nature has not been considered fully. Laurence et. al
16 (1973) suggested that $\text{Br}_2^{\bullet-}$ and $\text{Cl}_2^{\bullet-}$, generated by short duration (< 0.1 second) flash photolysis
17 of trihalide ions, oxidized $\text{Mn}^{2+}(\text{aq})$ at an extremely low pH (~1), and $\text{Mn}^{3+}(\text{aq})$ was proposed to
18 form rather than Mn(IV) oxide solids.¹⁸ Nevertheless, $\text{Mn}^{3+}(\text{aq})$ is not stable at circumneutral pH
19 in the absence of a ligand,¹⁹ so it is unclear whether these reactions can occur under
20 environmentally relevant pH conditions. Further, it is unknown whether reactive halogen radicals
21 can facilitate the oxidation of $\text{Mn}^{2+}(\text{aq})$ and form nanoscale Mn(IV) oxide solids as the final
22 products for a longer light illumination time rather than within one second.
23
24
25
26
27
28
29
30
31
32
33
34
35
36
37
38
39
40
41
42

43 Here, we show previously unknown effects of reactive halogen radicals on the oxidation of
44 $\text{Mn}^{2+}(\text{aq})$ and the fast kinetics of nanoscale Mn(IV) oxide solids formation. Reactive oxygen
45 species (ROS), including $\text{O}_2^{\bullet-}$ and $\bullet\text{OH}$, were produced during the photolysis of solution containing
46 nitrate.²⁰ When halides were present in the solution, reactive halogen radicals can be generated by
47 reactions between the halides and $\bullet\text{OH}$, increasing the oxidation rate of Mn^{2+} and also increasing
48 the rate and extent of Mn oxide nanosheets formation, compared with the rates of phenomena in
49
50
51
52
53
54
55
56
57
58
59
60

1
2
3 the absence of halides. More Mn^{2+} was oxidized by Br radicals (Br^\bullet and $\text{Br}_2^{\bullet-}$) generated from 1
4 mM NaBr than by Cl radicals (Cl^\bullet and $\text{Cl}_2^{\bullet-}$) generated from 500 mM NaCl. In addition, δ - MnO_2
5
6 nanosheets were formed by reactive halogen species. The crystallinity of the formed Mn oxide
7
8 nanosheets was affected by the ionic strength. This newly discovered reaction mechanism between
9
10 $\text{Mn}^{2+}(\text{aq})$ and reactive halogen radicals under environmental relevant conditions can advance our
11
12 understanding of nanoscale Mn oxide solids formation in the environment, and can help to predict
13
14 its redox activities, such as scavenging and oxidation of heavy metals (As, Pb, and Cr) and
15
16 geochemical elements (S, N, and P).
17
18
19
20
21

22 **2. Materials and methods**

23 **2.1 Chemicals and materials**

24
25
26 All chemicals used in this study were at least American Chemical Society grade. Manganese
27
28 chloride (MnCl_2 , 97%, anhydrous) was purchased from Beantown Chemical Co. (NH, USA).
29
30 Crystal sodium nitrate (NaNO_3 , $\geq 99.0\%$) was obtained from Avantor Performance Materials,
31
32 Inc. (PA, USA). Leucoberbelin blue I (LBB, 65%), potassium permanganate (KMnO_4 , $> 99\%$),
33
34 sodium sulfate (Na_2SO_4 , $\geq 99\%$), Sodium bromide (NaBr , $\geq 99.99\%$), superoxide dismutase
35
36 bovine (SOD, $> 90\%$), and 2-bromoacetophenone (BrAP, $> 98\%$) were purchased from Sigma-
37
38 Aldrich. Sodium hydroxide (NaOH , $> 97\%$) and sodium chloride (NaCl , $> 99\%$) were bought from
39
40 VWR International LLC. Deionized (DI) water (resistivity $\geq 18.2 \text{ M}\Omega\cdot\text{cm}$, Barnstead Ultrapure
41
42 water systems) was used to prepare the solutions for all experiments. $0.2 \mu\text{m}$
43
44 polytetrafluoroethylene (PTFE) membrane was bought from VWR International, LLC.
45
46
47
48
49
50
51
52
53
54
55
56
57
58
59
60

2.2 Photo-oxidation experiments

Photolytic experiments for Mn^{2+} oxidation were carried out in a 150 mL quartz reactor under a 450 W Xe-arc lamp (Newport 6279NS) equipped with a water optical filter to remove infrared light. The lamp provided stable light exposure with an irradiance intensity of $\sim 3.7 \text{ kW/m}^2$. The light spectrum of xenon arc lamp is shown in Fig. S1. Although the high irradiance intensity helped accelerate the reaction, the mechanism presented in this work is still representative of that under sunlight conditions. The effects of light intensity on the photolysis of nitrate and subsequent Mn^{2+} oxidation merit systematic future studies. Solutions of MnCl_2 , NaNO_3 , NaBr , NaCl , and SOD were exposed to the light for 6 hours.

0.1 mM MnCl_2 was used as the Mn source. The concentrations of dissolved Mn in natural waters can range from 10 $\mu\text{g/L}$ to 10,000 $\mu\text{g/L}$ (0.18 μM –0.18 mM).²¹⁻²³ Mandernack et al. examined Mn oxide mineral formation under environmentally relevant Mn concentrations of 10 μM –10 mM.²⁴ The Mn^{2+} concentrations used in this study might be higher than those in natural surface waters, however, these results can be useful in understanding diverse geochemical situations. In addition, 1 mM NaNO_3 was used in this study. According to a 2011 World Health Organization report on nitrate and nitrite in drinking water, in 1986, nitrate concentrations higher than 44 mg/L (0.71 mM) were detected in many surface water supplies.²⁵ Nitrate concentration can reach high levels in industrial areas or from contamination by human or animal wastes. For example, nitrate concentration can easily come up to several hundred mg/L (several mM) due to agricultural activities.²⁵ In addition, the ammonium in Marcellus and Fayetteville hydraulic fracturing flowback fluids can reach 420 mg/L (30 mM),⁴ and it can be further converted to nitrate.

To study the effects of different reactive halogen radicals on Mn oxidation, 1 mM NaBr and 500 mM NaCl were added either separately or together into a solution. These halide concentrations

1
2
3 represent a highly saline aqueous environment, including seawater and other water bodies with
4 similar concentrations. Adding 500 mM NaCl into 1 mM NaBr greatly increased ionic strength
5 (IS) of the solution. Thus, for better comparison the same IS was maintained between different
6 experimental conditions. Although others have substituted sodium perchlorate (NaClO₄) for NaCl
7 to maintain the same IS and Na⁺ concentration in a solution,⁶ NaClO₄ was not used in this study
8 because it could oxidize Mn²⁺ during photolysis by forming O₂^{•-}, even without nitrate (Fig. S2).
9 Instead, Na₂SO₄ was used to control the IS. To scavenge O₂^{•-}, 0.5 μM SOD was utilized. We did
10 not consider another halide ion, such as iodine, in this study because of its low concentrations in
11 seawater (450 to 500 nM)²⁶ and in contaminated surface waters from the brine treatment disposal
12 sites for hydraulic fracturing (e.g., in Pennsylvania hydraulic fracturing site, [I⁻] ≤ 7.9 μM, [Cl⁻]
13 = 1.7 M, [Br⁻] = 0.5 mM)⁴.
14
15
16
17
18
19
20
21
22
23
24
25
26
27
28

29 Based on the water quality criteria set by the U.S. Environmental Protection Agency (EPA),
30 freshwater pH ranges from 6.5 to 9.^{27, 28} To mimic environmentally relevant conditions, in this
31 study, the initial pH value was adjusted to 9.0 ± 0.1 using 10 mM NaOH and the pH decreased
32 within 6 hours as the Mn oxide solids formed. To understand the pH of the reaction systems, the
33 pH values were continuously monitored. No pH buffer was utilized to maintain the pH, because
34 Mn^{3+(aq)} forms strong complexation with pH buffers, such as pyrophosphate, EDTA, and citrate.
35
36
37
38
39
40
41
42
43
44
45
46
47
48
49
50
51
52
53
54
55
56
57
58
59
60

29, 30 The presence of pyrophosphate also affected the crystalline structure, morphology, and
oxidation kinetics of MnO₂.²⁹ In addition, carbonate ions were not used to control the pH because
they can react with •OH and reactive halogen radicals to form carbonate radicals,^{31, 32} which would
affect Mn^{2+(aq)} oxidation processes. After 6 hr of reaction, the solution pH dropped to the range
of 5–7, as shown in Fig. 2B and S2. As proved in our previous study, the pH drop was due mainly
to the formation of Mn oxide solids rather than CO₂ dissolution.¹⁷ As shown in Fig. 2A(5), during

1
2
3 the photolysis of 0.1 mM MnCl₂, 1 mM NaNO₃, and 0.5 μM SOD, O₂^{•-} was scavenged by SOD,
4
5 but •OH and dissolved CO₂ from air were still present in the solution and could form carbonate
6
7 radicals. However, no Mn oxidation was observed. Thus, we expect that the concentration of CO₂
8
9 from dissolution in air in 6 hr was not sufficient to play an important role in generating carbonate
10
11 radicals to induce Mn oxidation. In addition, this CO₂ dissolution process occurred under all
12
13 experimental conditions and was offset when the results were compared. So the effect of carbonate
14
15 radicals on Mn oxidation was not considered in this study.
16
17
18
19

20 **2.3 Quantification of formed nanoscale Mn oxide solids**

21
22 Concentrations of MnO₂ were quantified by using 0.004 % (w/v) LBB as reported before.^{17, 33, 34}
23
24 LBB reduced the high oxidation states of Mn(IV) and (III) in Mn oxide solids to aqueous Mn²⁺,
25
26 and then displayed a blue color (Fig. S3B). The intensity of oxidized LBB at 625 nm was
27
28 proportional to the concentration of Mn oxide solids. For LBB analyses, different concentrations
29
30 of KMnO₄ solutions were used to obtain a linear calibration curve. In these measurements, LBB
31
32 analyses cannot distinguish whether the detected oxidized Mn came from solid phase of Mn oxides
33
34 or aqueous oxidized Mn. Thus, 0.2 μm PTFE membrane was used to filter out the formed Mn
35
36 oxide solids and leave aqueous oxidized Mn in the solution. In this way, the existence of aqueous
37
38 oxidized Mn can be quantified by measuring the solutions after membrane filtration.
39
40
41
42
43

44 **2.4 Phase characterization of Mn oxide solids**

45
46 Photochemically-assisted synthesized solid MnO₂ products were collected by centrifugation at
47
48 10,000 rpm for 30 min. To remove impurities from the liquid supernatant, the solid products were
49
50 sequentially washed, resuspended in DI water, and centrifuged five times at 5,000 rpm for 5 min.
51
52 The resulting solid products were dried at room temperature for further characterization.
53
54
55
56
57
58
59
60

1
2
3 To identify the mineral phase of Mn oxides samples, we used high-resolution X-ray diffraction
4 (HRXRD, Bruker D8 Advance X-ray diffractometer with Cu K α radiation ($\lambda = 1.5418 \text{ \AA}$)).
5
6 Because of its low saturation index (SI) of -1.20 and solubility product constant (k_{sp}) of $1.6 \times 10^{-}$
7
8 $^{13,35} \text{Mn(OH)}_2$ (s) was not expected to form under above experimental conditions. MINEQL+
9
10 Version 4.6 was used to calculate the saturation indices for typical Mn(III)/Mn(IV) oxides based
11
12 on pH ranging from pH 9 to 6. Common Mn oxide minerals, for example, birnessite ($\delta\text{-MnO}_2$),
13
14 pyrolusite ($\beta\text{-MnO}_2$), hausmannite (Mn_3O_4), and manganite (MnOOH) have SI values of 9.48–
15
16 5.89, 11.54–7.95, 15.26–4.16, and 6.96–3.29, respectively, making them possible precipitates.
17
18
19
20
21

22 Mn oxidation states in the Mn oxides samples were identified by X-ray photoelectron
23
24 spectroscopy (XPS, PHI 5000 VersaProbe II, UlvacPHI with monochromatic Al K α radiation
25
26 (1486.6 eV)). The C 1s peak (284.8 eV) was employed as the reference peak. To determine the
27
28 ratio of Mn(II), Mn(III) and Mn(IV), the Mn 2p $_{3/2}$ spin orbit was fitted with Mn(II) (640.8eV),
29
30 Mn(III) (641.8 eV) and Mn(IV) (642.2 eV) by the Gauss-Lorentz fitting method. Sources for the
31
32 fitting reference values of Mn(II), Mn(III), and Mn(IV) are listed in Table S1. An environmental
33
34 scanning electron microscope (ESEM, ThermoFisher Quattro S) with an energy dispersive X-ray
35
36 spectrometer (EDX) was used to characterize the surface morphology and material composition.
37
38 Mn oxides samples were placed on a silicon wafer and visualized at a 10 mm working distance
39
40 with a 10 kV accelerating voltage.
41
42
43
44

45 To characterize the crystalline phases and morphology of Mn oxide solids, high resolution
46
47 transmission electron microscopy (HRTEM, JEOL-2100F) was used. The Mn oxide solids were
48
49 well dispersed by sonication for about 15 min. Then a droplet of the suspension was placed on an
50
51 ultrathin lacey carbon film coated-Cu grid (LC400-Cu-UL, Electron Microscopy Science, PA) for
52
53 imaging. Lattice fringes and selective area electron diffraction images were obtained to identify
54
55
56
57
58
59
60

1
2
3 the phases of Mn oxide solids. To measure the height (thickness) of MnO₂ nanosheets, tapping
4 mode atomic force microscopy (AFM) using a Nanoscope V multimode scanning probe
5 microscope (SPM, Veeco Inc., NY) in air was used. To measure the hydrodynamic diameter and
6 zeta potential of Mn oxide nanosheets in solutions, a Zetasizer Nano (Malvern Nano ZS) was used.
7
8
9

10 11 12 13 **2.5 Alternative method to generate Br radicals**

14
15
16 Photolysis of BrAP was used in an alternative method to generate Br radicals using a solution of
17 0.1 mM MnCl₂, 1 mM BrAP, and 0.5 μM SOD under photolysis. Mn oxide concentration and pH
18 were measured every minute. At least duplicate tests were conducted for each condition.
19
20
21
22

23 **3. Results and Discussion**

24 25 26 **3.1 ROS Responsible for Mn²⁺ oxidation**

27
28 Fig. 1A shows the reaction pathways that generate nitrogen oxide radicals (NO• or NO₂•), oxide
29 radical anion (O^{•-}), O₂^{•-}, and •OH during nitrate photolysis.²⁰ Among these products, O₂^{•-} and •OH
30 are the most common and most strongly reactive oxidants. We recently proved that the production
31 of ROS by nitrate photolysis can lead to fast oxidation of Mn²⁺ to nanoscale Mn oxide solids by
32 O₂^{•-}, even without organics or microorganisms.¹⁷ In the current study, we found that a solution
33 containing 0.1 mM MnCl₂ and 1 mM NaNO₃ at initial pH 9 changed solution color from
34 transparent to yellowish (Fig. S3A). Using LBB analysis, about 13.4 ± 1.0 μM of Mn oxide solids
35 (based on Mn(IV) oxidation state) were formed within 6 hr reaction, as shown in Fig. 2A(2). With
36 0.5 μM of SOD, a O₂^{•-} scavenger, no Mn oxidation was observed (Fig. 2A(5)), confirming that
37 O₂^{•-} radicals are majorly responsible for Mn oxidation, which is similar with biotic Mn oxidation
38 by extracellular O₂^{•-} radicals¹³⁻¹⁶. We have systematically proved •OH radicals have little
39 contribution for Mn oxide formation in our previous study.³³ An addition of *tert*-butyl alcohol, a
40
41
42
43
44
45
46
47
48
49
50
51
52
53
54
55
56
57
58
59
60

1
2
3 scavenger of $\cdot\text{OH}$ did not suppress Mn oxide formation and indeed increased the oxidation,
4 supporting that Mn^{2+} is majorly oxidized by $\text{O}_2^{\cdot-}$ rather than $\cdot\text{OH}$.^{17, 33} While $\cdot\text{OH}$ radicals are
5 powerful oxidants, they have a much shorter diffusion length and half-life (nanoseconds)
6 compared with $\text{O}_2^{\cdot-}$ (seconds).^{36, 37} These limitations may influence Mn^{2+} oxidation by $\cdot\text{OH}$. When
7 the pH became lower, slower Mn oxidation was observed. Mn oxidation was preferred at higher
8 pH,³⁸ and the decay of $\text{O}_2^{\cdot-}$ can be faster at lower pH values, inhibiting Mn oxidation.³⁹

17 **3.2 Faster Mn^{2+} oxidation in the presence of bromide radicals**

19
20 Interestingly, in the presence of an additional 1 mM NaBr during nitrate photolysis, 62% more
21 $\text{Mn}^{2+}(\text{aq})$ was oxidized within 6 hr of reaction than that without NaBr (Fig. 2A(1)). Also, the pH
22 of a solution of 0.1 mM MnCl_2 , 1 mM NaNO_3 , and 1 mM NaBr decreased to ~ 5.0 by 6 hr reaction
23 (Fig. 2B), faster than that without NaBr (decreased to $\sim \text{pH } 6.0$), due to the facilitated generation
24 of Mn oxide solids. Fig. 2A(3) shows that Mn oxide solids formed even in a solution of 0.1 mM
25 MnCl_2 , 1 mM NaNO_3 , 1 mM NaBr, and 0.5 μM SOD, indicating that new oxidant species, rather
26 than $\text{O}_2^{\cdot-}$, were oxidizing $\text{Mn}^{2+}(\text{aq})$ to Mn oxide solids. We hypothesized that the additional Mn
27 oxidation could be attributed to the Br radicals formed by the reactions between $\cdot\text{OH}$ and Br^- . To
28 test this hypothesis, Na_2SO_4 was substituted for NaBr. Mn oxidation was not detected in a solution
29 of 0.1 mM MnCl_2 , 1 mM NaNO_3 , 1 mM Na_2SO_4 , and 0.5 μM SOD (Fig. 2A(4)). Additionally, no
30 Mn oxidation was observed in a solution of 0.1 mM MnCl_2 and 1 mM NaBr during photolysis
31 (Fig. S4A), indicating that NaBr cannot directly oxidize Mn^{2+} during photolysis. Thus, we
32 concluded that the additional Mn oxide solids are formed by Br radicals generated from the series
33 of reactions between NaBr and $\cdot\text{OH}$ (Fig. 1B). In the presence of Br radicals, 62% more Mn
34 oxidation was observed than that without Br^- , suggesting that abiotic Mn oxidation by reactive
35 radicals makes a significant contribution in nature. Halogen radicals can transform to nonradical
36
37
38
39
40
41
42
43
44
45
46
47
48
49
50
51
52
53
54
55
56
57
58
59
60

1
2
3 halogen oxidants (e.g., hypohalous acid, HOX), as shown in Equations 1 and 2 below,⁵ which can
4
5 then oxidize Mn²⁺ to Mn oxide solids.⁴⁰
6



9
10
11
12 However, such nonradical oxidants are not the major loss pathways for halogen radicals.⁵ HOX
13
14 can further react with O₂^{•-} to form [•]OH and X⁻,⁴¹ and thus HOX is unlikely to be a major cause of
15
16 Mn²⁺ oxidation.
17
18

19
20 In addition to Mn oxide solid phase formation, we further explored whether reactive halogen
21
22 radicals can oxidize Mn²⁺ to stable aqueous species, i.e., Mn(III)–halide complexation at
23
24 circumneutral pH. Aqueous samples were taken every hour from a solution containing 0.1 mM
25
26 MnCl₂, 1 mM NaNO₃, 1 mM NaBr, and 0.5 μM SOD. The samples were filtered through 0.2 μm
27
28 polytetrafluoroethylene (PTFE) filters three times to remove all Mn oxide solids in the solution
29
30 before measuring the Mn(III)–halide concentration. This filtration is necessary because the LBB
31
32 method only detects the oxidized Mn concentration but cannot distinguish whether it is in the solid
33
34 or aqueous phase. In the filtered solution (Fig. S4B), no oxidized aqueous Mn species was detected
35
36 via the LBB method, which confirmed the absence of aqueous Mn(III) complex in the solution.
37
38 The initial pH of the solution also affected the Mn oxidation rate (Fig. S5). Compared with an
39
40 initial pH of 9, a slower Mn oxidation rate was observed at an initial pH of 6.
41
42
43
44
45

46 **3.3 Validation of Mn oxidation by Br radicals**

47
48 To further validate the finding that Mn²⁺ can be oxidized by reactive halogen radicals, BrAP was
49
50 used to directly produce Br[•] by photolysis (Fig. 3),⁴² rather than generating it from the reaction
51
52 between halides and [•]OH formed by nitrate photolysis. Because the generated Br[•] can rapidly react
53
54 with OH⁻ to form [•]OH, and further produce to O₂^{•-} via chain reactions (Fig. 3A),⁶ the potentially
55
56
57
58
59
60

1
2
3 formed $O_2^{\bullet-}$ was scavenged by adding SOD. Fig. 3B shows the results of 4 min of photolysis of a
4 solution containing 0.1 mM $MnCl_2$, 1 mM BrAP, and 0.5 μM SOD. About 3 μM Mn oxide solids
5
6 (based on Mn(IV) oxidation state) were produced, and the solution pH dropped from 5.5 to 4.4,
7
8 further proving that Mn^{2+} was indeed oxidized by reactive halogen radicals. Taken together, the
9
10 above results clearly demonstrated that reactive halogen radicals can contribute significantly to the
11
12 formation of Mn oxide solids from aqueous Mn^{2+} .
13
14
15
16

17 **3.4 The different contributions of Cl and Br radicals to Mn^{2+} oxidation**

18
19
20 While $\bullet OH$ had little contribution to oxidizing $Mn^{2+}(aq)$ to Mn oxide solids, $\bullet OH$ can react with
21
22 halide ions (Cl^- or Br^-) to form reactive halogen radicals that oxidize $Mn^{2+}(aq)$. As shown in Fig.
23
24 1B, halide ions can be oxidized to monatomic radicals ($Cl\bullet$ or $Br\bullet$) by $\bullet OH$.⁴³⁻⁴⁵ In addition, diatomic
25
26 radicals ($Cl_2^{\bullet-}$, $Br_2^{\bullet-}$, or $ClBr^{\bullet-}$) can be generated.⁴³⁻⁴⁵ To understand the effects of different halide
27
28 ions contribution and different ion concentrations on Mn oxidation, we tested Mn oxidation using
29
30 a solution containing 0.1 mM $MnCl_2$, 1 mM $NaNO_3$, 1 mM NaBr, or/and 500 mM NaCl. These
31
32 NaBr and NaCl concentrations were chosen as a representative condition to study a highly saline
33
34 aqueous environment. The IS of the solution was greatly changed in the solution containing 0.1
35
36 mM $MnCl_2$ and 1 mM $NaNO_3$, and 500 mM of NaCl (IS ~500 mM), compared with that of a
37
38 solution containing 0.1 mM $MnCl_2$ and 1 mM $NaNO_3$, and 1 mM NaBr (IS ~2 mM). As a result,
39
40 Na_2SO_4 was added to maintain the same IS between different experimental conditions for better
41
42 comparison. A high IS of 500 mM strongly hindered the Mn oxidation process. Only ~7 μM Mn^{2+}
43
44 was oxidized by $O_2^{\bullet-}$ after 6 hr reaction during the photolysis of a solution containing 0.1 mM
45
46 $MnCl_2$, 1 mM $NaNO_3$, and 166.7 mM Na_2SO_4 (IS ~500 mM) (Fig. 4A(4)), which was only a half
47
48 the Mn^{2+} oxidation amount in the solution without Na_2SO_4 at a lower IS (IS ~1 mM) (Fig. 2A(2)).
49
50
51
52
53
54
55 Because the higher IS reduced the activity coefficient and the saturation index of precursors with
56
57
58
59
60

1
2
3 respect to forming Mn oxide solids, it provided a lower thermodynamic driving force for Mn oxide
4 nucleation and could result in a slower formation kinetics.
5
6

7
8 The contributions of Cl^- and Br^- to Mn oxidation differed due to their different concentrations
9 in surface water and their efficacies in reactivity. Although NaBr had a 500-fold lower
10 concentration than NaCl, at the same IS, more Mn^{2+} was oxidized by Br radicals generated from
11 NaBr than by Cl radicals generated from NaCl, as seen in Fig. 4A (2 and 3). Most of the $\text{BrOH}^{\cdot-}$,
12 the intermediate radical generated from the reaction between $\cdot\text{OH}$ and Br^- , as shown in Fig. 1B,
13 can further transform to other reactive halogen radicals, such as Br^{\cdot} and $\text{Br}_2^{\cdot-}$,^{5,44,46} oxidizing Mn^{2+} .
14 On the other hand, for Cl radicals, more than 99% of $\text{ClOH}^{\cdot-}$ reverted to $\cdot\text{OH}$ and Cl^- instead of
15 forming Cl^{\cdot} and $\text{Cl}_2^{\cdot-}$.^{5,47-49} Thus, Cl radicals caused less Mn^{2+} oxidation.
16
17
18
19
20
21
22
23
24
25
26

27 When 1 mM NaBr and 500 mM NaCl were dissolved together (Fig. 4A(1)), more Mn oxide
28 formation was observed than that from adding 1 mM NaBr or 500 mM NaCl separately (Fig. 4A(2)
29 or (3)) at the same IS. The higher oxidation of Mn^{2+} could result from the sum of Br and Cl radicals
30 compared with single halide radicals. In addition, the promoted Mn oxide formation could result
31 from the reaction product in the co-presence of Br^- and Cl^- . When Br^- and Cl^- co-existed, $\text{ClBr}^{\cdot-}$
32 can be formed at a higher rate constant than the formation rates of Br^{\cdot} and $\text{Br}_2^{\cdot-}$ from a Br^- only
33 system.⁵ Thus, we postulated that the coexistence of Br^- and Cl^- in our experimental system would
34 generate $\text{ClBr}^{\cdot-}$, which can also oxidize Mn^{2+} to Mn oxide solids faster.
35
36
37
38
39
40
41
42
43
44
45

46 **3.5 Characterization of MnO_2 solids formed by $\text{O}_2^{\cdot-}$ or/and Br radicals**

47
48 HRXRD was used to obtain the crystalline structure of Mn oxide formed by Br radicals, $\text{O}_2^{\cdot-}$, and
49 Br radicals together with $\text{O}_2^{\cdot-}$, with the results shown in Fig. 5A. The 2θ XRD peaks at about 12.3° ,
50 24.7° , and 36.7° indicated that birnessite, $\delta\text{-MnO}_2$ (ICDD PDF-4 #00-043-1456), was formed in
51 all three above conditions. $\delta\text{-MnO}_2$ produced by Br radicals was quite amorphous and less
52
53
54
55
56
57
58
59
60

1
2
3 crystalline than that formed by $O_2^{\bullet-}$. δ -MnO₂ synthesized in the co-presence of Br radicals and
4
5 $O_2^{\bullet-}$ presented the highest crystallinity. HRTEM images (Fig. 5B) show a thin, nanosheet
6
7 morphology, with the edge rolling up due to high surface tension. In Fig. 5C, crystalline lattices
8
9 with d-spacings of 0.32 nm and 0.25 nm indicated the (002) and (110)/(200) planes of δ -MnO₂,
10
11 respectively. The (001) interlayer plane was observed with a 0.51 nm d-spacing, which was smaller
12
13 than that calculated from XRD measurement (\sim 0.7 nm), probably owing to the loss of interlayer
14
15 water in the high vacuum environment of TEM.⁵⁰ The selected area electron diffraction (SAED)
16
17 patterns in the Fig. 5B inset were also consistent with the d-spacings of the (001), (002), and
18
19 (110)/(200) planes, which further confirmed the formation of δ -MnO₂. The AFM images shown
20
21 in Fig. S6 were used to measure the height (thickness) of the MnO₂ nanosheets. The lateral
22
23 dimension of the MnO₂ solids was about 1.5 μ m and the thickness was 4–5 nm, values that
24
25 confirmed its nanosheet morphology. Because a single layer of MnO₂ is \sim 0.7 nm thick in ambient
26
27 pressure, a 4–5 nm thickness corresponds to 6–7 layers. The hydrodynamic diameters and zeta
28
29 potential value of the Mn oxide solids were measured by electrophoretic mobility measurements
30
31 to provide additional physicochemical information. The hydrodynamic diameter of MnO₂ solids
32
33 formed *via* 6 hr photolysis of a solution containing 0.1 mM MnCl₂, 1 mM NaNO₃, and 1 mM NaBr
34
35 was 2540 ± 166 nm, which reflects the average lateral dimension sizes of MnO₂ nanosheets. The
36
37 formed MnO₂ nanosheets had a negative zeta potential value of -18.9 ± 0.4 mV. The ESEM image
38
39 shows a rough layered morphology, and EDX results suggest a slight percentage (0.2 %) of Na⁺
40
41 incorporation into the structure (Fig. S7). The XPS image in Fig. 5D suggested that formed Mn
42
43 oxide solids mainly contained Mn(III) and Mn(IV), with a very small fraction of Mn(II). In general,
44
45 Mn oxidation states did not show much practical difference between Mn oxide solids formed with
46
47 and without NaBr. Slightly higher proportions of Mn(II) and Mn(III) were detected in δ -MnO₂
48
49
50
51
52
53
54
55
56
57
58
59
60

1
2
3 produced in the presence of NaBr, resulting in a slightly lower Mn average oxidation state (3.67)
4 in Fig. 5F than that in the absence of NaBr (3.73) in Fig. 5E. Please note that the Mn oxide solids
5 generation results shown in Fig. 2A were calculated by the LBB method, which assumed that the
6 Mn oxide solids consisted of only Mn(IV). Because the average oxidation state of Mn was lower
7 than 4 in the XPS results, the actual concentrations of Mn oxide solids could be higher than the
8 values in Fig. 2A.
9

10 **3.6 Effects of $O_2^{\cdot-}$ or/and reactive halogen radicals on Mn^{2+} oxidation and subsequent Mn** 11 **oxide nanosheet formation** 12 13

14 To investigate the singular contributions of reactive halogen radicals (Cl and Br radicals) to Mn
15 oxidation without $O_2^{\cdot-}$, SOD was added to scavenge $O_2^{\cdot-}$ in the solution. As shown in Fig. 4A(6),
16 without any halides, no Mn oxidation was observed during the photolysis of a solution containing
17 0.1 mM $MnCl_2$, 1 mM $NaNO_3$, 166.7 mM Na_2SO_4 , and 0.5 μM SOD, because neither reactive
18 halogen radicals nor $O_2^{\cdot-}$ were present to oxidize Mn^{2+} . Substituting 1 mM NaBr and 500 mM
19 NaCl for the 166.7 mM Na_2SO_4 caused the generation of reactive halogen radicals and Mn oxide
20 solids formation (Fig. 4A(5)). Fig. 4B displays the Mn^{2+} oxidation amounts after 6 hr reaction
21 under different conditions at low or high IS: $O_2^{\cdot-}$, Br and/or Cl radicals, and $O_2^{\cdot-}$ with Br and/or
22 Cl radicals. At the same IS (the dashed box in Fig. 4B), the contribution of $O_2^{\cdot-}$, Br radicals, and
23 Cl radicals to Mn oxide solids generation can be fairly compared. More Mn oxide nanosheets were
24 formed during nitrate photolysis in the presence of additional halide ions. As seen in Fig. S8, for
25 all experiments at about 500 mM IS, the solution pH changed with time, but all showed the same
26 pH trend, decreasing from an initial pH 9.0 to pH 7.0–6.0 after 6 hr of photolysis. A slightly faster
27 pH drop was observed with a larger amount of Mn oxide nanosheet formation.
28
29
30
31
32
33
34
35
36
37
38
39
40
41
42
43
44
45
46
47
48
49
50
51
52
53
54
55
56
57
58
59
60

1
2
3 In the coexistence of Cl and Br radicals, the HRXRD results in Fig. 6A(1) and (3) confirmed
4 that Mn oxide had a higher crystallinity than that produced by Br radicals, as shown in Fig. 6A(2)
5 and (4), respectively. This finding suggested that higher IS promoted the crystallization of Mn
6 oxide, although slower kinetics for Mn^{2+} formation by Cl radicals together with Br radicals was
7 observed than for Br radicals alone (navy blue vs. orange and black vs. blue in Fig. 4B). Based on
8 XPS analysis, the average Mn oxidation states of Mn oxide produced by $\text{O}_2^{\cdot-}$ and/or Br radicals
9 was 3.68–3.73 (Fig. 5D–F) under low IS conditions (i.e., less than 2 mM), while they decreased
10 to 3.57–3.63 (Fig. 6B) under high IS conditions (~500 mM) because of larger Mn(III) and smaller
11 Mn(IV) portions. The insignificantly lower Mn oxidation states may result from charge
12 compensation for more Na^+ incorporation into the structure of Mn oxide nanosheets (3.4% of Na^+ ,
13 Fig. 6D) at high IS compared with that at low IS (0.2% of Na^+ , Fig. S7). The ESEM image in Fig.
14 6C showed that Mn oxide samples presented rumpled and wrinkled surface morphology. Zhang et
15 al. (2018) reported that intercalated Na^+ tended to shift and coordinate with two unsaturated O
16 from the MnO_6 layer via strong electrostatic interactions rather than staying in between two MnO_6
17 layers to balance the interactions, resulting in unbalanced supporting interstitial distances between
18 MnO_6 layers and causing a rough surface.⁵¹

41 **4. Conclusions and environmental implications**

42
43
44 Here we show the hitherto unexplored oxidation of Mn^{2+} by reactive halogen radicals. Compared
45 to the abiotic oxidation rate of Mn^{2+} without Br radicals, in the presence of Br radicals, the abiotic
46 oxidation rate of Mn^{2+} to Mn oxide nanosheets was greatly facilitated, exhibiting a 62% increase
47 within 6 hr. In the natural environment, NaBr had a much lower concentration than NaCl, however,
48 at the same experimental IS, more Mn^{2+} was oxidized by Br radicals generated from 1 mM NaBr
49 than by Cl radicals generated from 500 mM NaCl. δ - MnO_2 nanosheets were formed by reactive
50
51
52
53
54
55
56
57

1
2
3 halogen species, and increasing the IS caused more highly crystalline Mn oxides to form. Although
4
5 the pH, the concentrations of Mn^{2+} , nitrate, and halides, and the intensity of light illumination
6
7 obviously vary in different water bodies, this study provides a good starting point for
8
9 understanding how halogen radicals are generated and affect Mn^{2+} oxidation processes. This work
10
11 highlights the importance of underappreciated reactive halogen radicals in inorganic redox
12
13 reactions in aqueous environmental systems. In nature, reactive halogen radicals can be produced
14
15 *via* oxidation of halides by $\cdot\text{OH}$, $\text{SO}_4^{\cdot-}$, or triplet state dissolved organic matter ($^3\text{DOM}^*$).⁵ The
16
17 natural contribution of reactive halogen radicals to Mn^{2+} oxidation and MnO_2 formation merit
18
19 future systematic experiments. The redox reaction mechanism between reactive halogen radicals
20
21 and $\text{Mn}^{2+}(\text{aq})$ can be applicable to other redox-sensitive transition metal ions, such as Fe^{2+} , As^{3+} ,
22
23 and Cr^{3+} . Furthermore, the results are also critically valuable to understanding aerosol reactions
24
25 involving halides in the atmosphere. Halide ions are preferentially present at air-water interfaces
26
27 rather than in bulk solution,⁵² where surface halide ions can actively react with $\cdot\text{OH}$ to generate
28
29 halogen radicals.⁵³ In the atmosphere, this behavior can amplify the effects of reactive halogen
30
31 species on the oxidation of redox active metals, forming nanoscale mineral aerosols that can act as
32
33 cloud condensation nuclei and affect the albedo. Moreover, compared with bulk MnO_2 particles
34
35 that do not have any nanoscale planes or structures, nanoscale MnO_2 shows an improved catalytic
36
37 performance for electrochemical oxygen reduction.⁵⁴ This study suggests a novel,
38
39 environmentally-friendly, and facile pathway for the synthesis of MnO_2 nanosheets.

46 47 **Author contributions**

48
49 Z. G., C. S., and Y.-S. J. conducted the experiments. Z. G. and Y.-S. J. designed the experimental
50
51 setup and procedures and wrote the manuscript. All authors discussed the results and collectively
52
53 revised the manuscript.
54
55
56
57

Conflicts of Interest

The authors declare that they have no known competing financial interests or personal relationships that could have appeared to influence the work reported in this paper.

Acknowledgments

This work is supported by National Science Foundation's Environmental Chemical Sciences program (CHE-1905077). The authors would like to acknowledge the Institute of Materials Science & Engineering (IMSE) of Washington University in St. Louis for the use of XPS, ESEM, and TEM, Professor Kimberly Parker for providing suggestions, and Professor James C. Ballard for carefully reviewing the manuscript.

References

1. N. Voutchkov, Overview of seawater concentrate disposal alternatives, *Desalination*, 2011, **273**, 205-219.
2. C. Zhang, Y. Shi, L. Shi, H. Li, R. Li, S. Hong, S. Zhuo, T. Zhang and P. Wang, Designing a next generation solar crystallizer for real seawater brine treatment with zero liquid discharge, *Nat. Commun.*, 2021, **12**, 1-10.
3. K. B. Gregory, R. D. Vidic and D. A. Dzombak, Water management challenges associated with the production of shale gas by hydraulic fracturing, *Elements*, 2011, **7**, 181-186.
4. J. S. Harkness, G. S. Dwyer, N. R. Warner, K. M. Parker, W. A. Mitch and A. Vengosh, Iodide, bromide, and ammonium in hydraulic fracturing and oil and gas wastewaters: environmental implications, *Environ. Sci. Technol.*, 2015, **49**, 1955-1963.
5. K. Zhang and K. M. Parker, Halogen radical oxidants in natural and engineered aquatic systems, *Environ. Sci. Technol.*, 2018, **52**, 9579-9594.
6. K. M. Parker and W. A. Mitch, Halogen radicals contribute to photooxidation in coastal and estuarine waters, *Proc. Natl. Acad. Sci. U. S. A.*, 2016, **113**, 5868-5873.
7. K. M. Parker, E. S. Reichwaldt, A. Ghadouani and W. A. Mitch, Halogen radicals promote the photodegradation of microcystins in estuarine systems, *Environ. Sci. Technol.*, 2016, **50**, 8505-8513.
8. S. Cheng, X. Zhang, X. Yang, C. Shang, W. Song, J. Fang and Y. Pan, The multiple role of bromide ion in PPCPs degradation under UV/chlorine treatment, *Environ. Sci. Technol.*, 2018, **52**, 1806-1816.
9. C. R. Stephens, P. B. Shepson, A. Steffen, J. W. Bottenheim, J. Liao, L. G. Huey, E. Apel, A. Weinheimer, S. R. Hall and C. Cantrell, The relative importance of chlorine and bromine radicals in the oxidation of atmospheric mercury at Barrow, Alaska, *J. Geophys. Res. Atmos.*, 2012, **117**.
10. C. R. Myers and K. H. Nealson, Bacterial manganese reduction and growth with manganese oxide as the sole electron acceptor, *Science*, 1988, **240**, 1319-1321.
11. B. M. Tebo, J. R. Bargar, B. G. Clement, G. J. Dick, K. J. Murray, D. Parker, R. Verity and S. M. Webb, Biogenic manganese oxides: properties and mechanisms of formation, *Annu. Rev. Earth Planet. Sci.*, 2004, **32**, 287-328.
12. C. N. Butterfield, A. V. Soldatova, S.-W. Lee, T. G. Spiro and B. M. Tebo, Mn(II, III) oxidation and MnO₂ mineralization by an expressed bacterial multicopper oxidase, *Proc. Natl. Acad. Sci. U. S. A.*, 2013, **110**, 11731-11735.
13. D. Learman, B. Voelker, A. Vazquez-Rodriguez and C. Hansel, Formation of manganese oxides by bacterially generated superoxide, *Nat. Geosci.*, 2011, **4**, 95-98.
14. C. M. Hansel, C. A. Zeiner, C. M. Santelli and S. M. Webb, Mn(II) oxidation by an ascomycete fungus is linked to superoxide production during asexual reproduction, *Proc. Natl. Acad. Sci. U. S. A.*, 2012, **109**, 12621-12625.
15. D. Learman, S. Wankel, S. Webb, N. Martinez, A. Madden and C. Hansel, Coupled biotic–

- 1
2
3 abiotic Mn(II) oxidation pathway mediates the formation and structural evolution of
4 biogenic Mn oxides, *Geochim. Cosmochim. Acta*, 2011, **75**, 6048-6063.
- 5
6 16. J. M. Diaz, C. M. Hansel, B. M. Voelker, C. M. Mendes, P. F. Andeer and T. Zhang,
7 Widespread production of extracellular superoxide by heterotrophic bacteria, *Science*,
8 2013, 1237331.
- 9
10 17. H. Jung, T. S. Chadha, D. Kim, P. Biswas and Y.-S. Jun, Photochemically assisted fast
11 abiotic oxidation of manganese and formation of δ -MnO₂ nanosheets in nitrate solution,
12 *Chem. Commun.*, 2017, **53**, 4445-4448.
- 13
14 18. G. S. Laurence and A. T. Thornton, Kinetics of oxidation of transition-metal ions by
15 halogen radical anions. Part III. The oxidation of manganese(II) by dibromide and
16 dichloride ions generated by flash photolysis, *J. Chem. Soc., Dalton Trans.*, 1973, 1637-
17 1644.
- 18
19 19. G. Davies, Some aspects of the chemistry of manganese(III) in aqueous solution, *Coord.*
20 *Chem. Rev.*, 1969, **4**, 199-224.
- 21
22 20. J. Mack and J. R. Bolton, Photochemistry of nitrite and nitrate in aqueous solution: a review,
23 *J. Photochem. Photobiol. A: Chem.*, 1999, **128**, 1-13.
- 24
25 21. WHO, *Concise international chemical assessment document 12, Manganese and its*
26 *compounds*, World Health Organization, 1999.
- 27
28 22. WHO, *Concise international chemical assessment document 63, Manganese and its*
29 *Compounds: Environmental Aspects*, World Health Organization, 2004.
- 30
31 23. M. Williams, G. D. Todd, N. Roney, J. Crawford, C. Coles, P. R. McClure, J. D. Garey, K.
32 Zaccaria and M. Citra, Toxicological profile for manganese, 2013.
- 33
34 24. K. W. Mandernack, J. Post and B. M. Tebo, Manganese mineral formation by bacterial
35 spores of the marine *Bacillus*, strain SG-1: Evidence for the direct oxidation of Mn(II) to
36 Mn(IV), *Geochim. Cosmochim. Acta*, 1995, **59**, 4393-4408.
- 37
38 25. WHO, *Nitrate and nitrite in drinking-water*, World Health Organization 2011.
- 39
40 26. R. Chance, A. R. Baker, L. Carpenter and T. D. Jickells, The distribution of iodide at the
41 sea surface, *Env. Sci. Process. Impact.*, 2014, **16**, 1841-1859.
- 42
43 27. EPA, *Quality criteria for water*, 1986.
- 44
45 28. EPA, pH, <https://www.epa.gov/caddis-vol2/caddis-volume-2-sources-stressors-responses-ph>,
46 (accessed January 18, 2021).
- 47
48 29. H. Jung, T. S. Chadha, Y. Min, P. Biswas and Y.-S. Jun, Photochemically-assisted
49 synthesis of birnessite nanosheets and their structural alteration in the presence of
50 pyrophosphate, *ACS Sustainable Chem. Eng.*, 2017, **5**, 10624-10632.
- 51
52 30. J. K. Klewicki and J. J. Morgan, Kinetic behavior of Mn(III) complexes of pyrophosphate,
53 EDTA, and citrate, *Environ. Sci. Technol.*, 1998, **32**, 2916-2922.
- 54
55 31. R. E. Huie, C. L. Clifton and P. Neta, Electron transfer reaction rates and equilibria of the
56 carbonate and sulfate radical anions, *International Journal of Radiation Applications and*
57 *Instrumentation. Part C. Radiation Physics and Chemistry*, 1991, **38**, 477-481.
- 58
59
60

- 1
2
3 32. S. Yan, Y. Liu, L. Lian, R. Li, J. Ma, H. Zhou and W. Song, Photochemical formation of
4 carbonate radical and its reaction with dissolved organic matters, *Water Res.*, 2019, **161**,
5 288-296.
6
7 33. Z. Gao, D. Zhang and Y.-S. Jun, Does *tert*-butyl alcohol really terminate the oxidative
8 activity of $\cdot\text{OH}$ in inorganic redox chemistry?, *Environ. Sci. Technol.*, 2021, **55**, 10442-
9 10450.
10
11 34. M. R. Jones, G. W. Luther III, A. Mucci and B. M. Tebo, Concentrations of reactive
12 Mn(III)-L and MnO₂ in estuarine and marine waters determined using spectrophotometry
13 and the leuco base, leucoberbelin blue, *Talanta*, 2019, **200**, 91-99.
14
15 35. R. K. Fox, D. F. Swinehart and A. Garrett, The equilibria of manganese hydroxide,
16 Mn(OH)₂, in solutions of hydrochloric acid and sodium hydroxide, *J. Am. Chem. Soc.*,
17 1941, **63**, 1779-1782.
18
19 36. M. Levy, P. P. Chowdhury and P. Nagpal, Quantum dot therapeutics: a new class of radical
20 therapies, *J. Biol. Eng.*, 2019, **13**, 48.
21
22 37. K. Krumova and G. Cosa, Overview of reactive oxygen species, 2016.
23
24 38. Z. Gao, J. Liu, C. Skurie, Y. Zhu and Y.-S. Jun, Photochemical reactions of dissolved
25 organic matter and bromide ions facilitate abiotic formation of manganese oxide solids,
26 *Water Res.*, 2022, 118831.
27
28 39. J. Ma, H. Zhou, S. Yan and W. Song, Kinetics studies and mechanistic considerations on
29 the reactions of superoxide radical ions with dissolved organic matter, *Water Res.*, 2019,
30 **149**, 56-64.
31
32 40. S. Allard, L. Fouche, J. Dick, A. Heitz and U. von Gunten, Oxidation of manganese(II)
33 during chlorination: role of bromide, *Environ. Sci. Technol.*, 2013, **47**, 8716-8723.
34
35 41. E. M. Rodríguez and U. von Gunten, Generation of hydroxyl radical during chlorination
36 of hydroxyphenols and natural organic matter extracts, *Water Res.*, 2020, **177**, 115691.
37
38 42. W. McGimpsey and J. Scaiano, Photochemistry of α -chloro- and α -bromoacetophenone.
39 Determination of extinction coefficients for halogen-benzene complexes, *Can. J. Chem.*,
40 1988, **66**, 1474-1478.
41
42 43. P. F. De Violet, Polyhalide radical anions as intermediates in chemistry, *Reviews of*
43 *Chemical Intermediates*, 1981, **4**, 121-169.
44
45 44. D. Zehavi and J. Rabani, Oxidation of aqueous bromide ions by hydroxyl radicals. Pulse
46 radiolytic investigation, *J. Phys. Chem.*, 1972, **76**, 312-319.
47
48 45. X.-Y. Yu and J. R. Barker, Hydrogen peroxide photolysis in acidic aqueous solutions
49 containing chloride ions. I. Chemical mechanism, *The Journal of Physical Chemistry A*,
50 2003, **107**, 1313-1324.
51
52 46. G. Merenyi and J. Lind, Reaction mechanism of hydrogen abstraction by the bromine atom
53 in water, *J. Am. Chem. Soc.*, 1994, **116**, 7872-7876.
54
55 47. G. Jayson, B. Parsons and A. J. Swallow, Some simple, highly reactive, inorganic chlorine
56 derivatives in aqueous solution. Their formation using pulses of radiation and their role in
57 the mechanism of the Fricke dosimeter, *J. Chem. Soc., Faraday Trans. 1 F*, 1973, **69**, 1597-

- 1
2
3 1607.
4
5 48. A. Grigor'ev, I. Makarov and A. Pikaev, Formation of Cl_2^- in the bulk of solution during
6 radiolysis of concentrated aqueous solutions of chlorides, *Khimiya Vysokikh Ehnergij*,
7 1987, **21**, 123-126.
8
9 49. U. K. Klänning and T. Wolff, Laser flash photolysis of HClO , ClO^- , HBrO , and BrO^- in
10 aqueous solution. reactions of Cl- and Br-atoms, *Ber. Bunsenge. Phys. Chem.*, 1985, **89**,
11 243-245.
12
13 50. J. Zhu, Q. Li, W. Bi, L. Bai, X. Zhang, J. Zhou and Y. Xie, Ultra-rapid microwave-assisted
14 synthesis of layered ultrathin birnessite $\text{K}_{0.17}\text{MnO}_2$ nanosheets for efficient energy storage,
15 *J. Mater. Chem. A*, 2013, **1**, 8154-8159.
16
17 51. T. Zhang, L. Liu, W. Tan, S. L. Suib, G. Qiu and F. Liu, Photochemical formation and
18 transformation of birnessite: Effects of cations on micromorphology and crystal structure,
19 *Environ. Sci. Technol.*, 2018, **52**, 6864-6871.
20
21 52. P. Jungwirth and D. J. Tobias, Ions at the air/water interface, *J. Phys. Chem. B*, 2002, **106**,
22 6361-6373.
23
24 53. E. Knipping, M. Lakin, K. Foster, P. Jungwirth, D. Tobias, R. Gerber, D. Dabdub and B.
25 Finlayson-Pitts, Experiments and simulations of ion-enhanced interfacial chemistry on
26 aqueous NaCl aerosols, *Science*, 2000, **288**, 301-306.
27
28 54. F. Cheng, Y. Su, J. Liang, Z. Tao and J. Chen, MnO_2 -based nanostructures as catalysts for
29 electrochemical oxygen reduction in alkaline media, *Chem. Mater.*, 2010, **22**, 898-905.
30
31
32
33
34
35
36
37
38
39
40
41
42
43
44
45
46
47
48
49
50
51
52
53
54
55
56
57
58
59
60

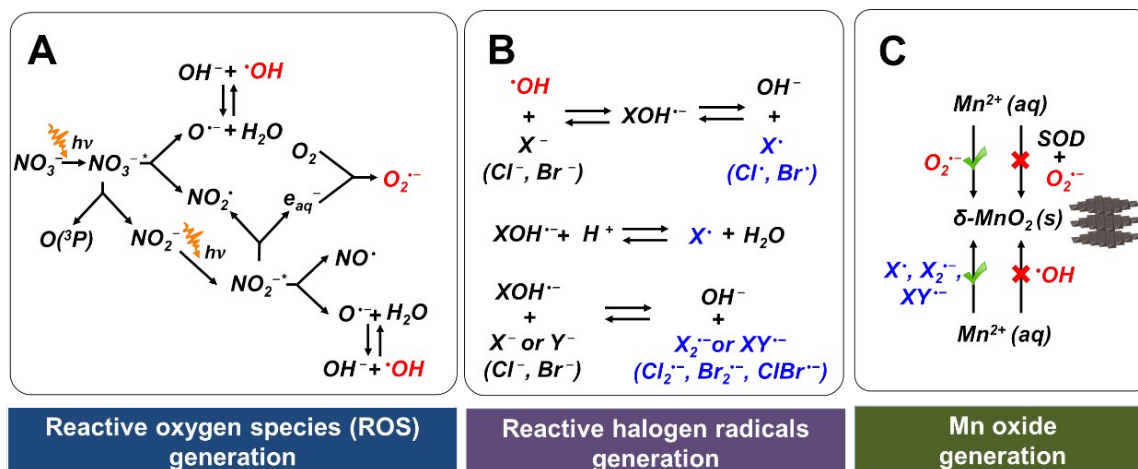


Figure 1. Schematics of the generation pathways of ROS and reactive halogen radicals, and Mn²⁺ oxidation pathways. (A) Chain reactions in the generation of O₂^{·-} and [·]OH during nitrate photolysis. (B) Chain reactions in the generation of reactive halogen radicals. (C) Mn²⁺(aq) oxidation by O₂^{·-} and reactive halogen radicals.

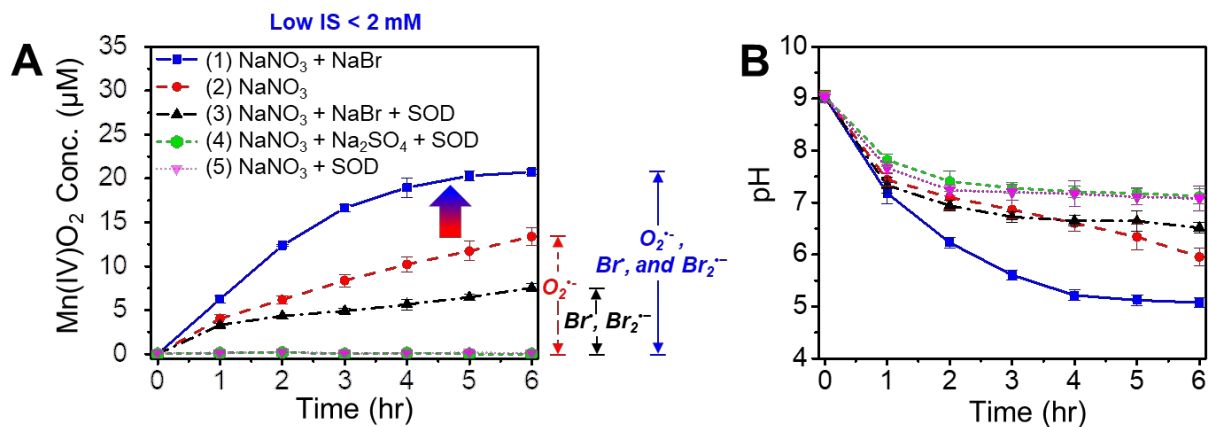


Figure 2. Oxidation of $\text{Mn}^{2+}(\text{aq})$ to Mn oxide solids by $\text{O}_2^{\bullet-}$ or/and Br radicals. (A) Oxidized Mn concentrations and (B) pH values during 6 hr of photolysis of solutions containing (1) 0.1 mM MnCl_2 , 1 mM NaNO_3 , and 1 mM NaBr ; (2) 0.1 mM MnCl_2 and 1 mM NaNO_3 ; (3) 0.1 mM MnCl_2 , 1 mM NaNO_3 , 1 mM NaBr , and 0.5 μM SOD; (4) 0.1 mM MnCl_2 , 1 mM NaNO_3 , 1 mM Na_2SO_4 , and 0.5 μM SOD; and (5) 0.1 mM MnCl_2 , 1 mM NaNO_3 , and 0.5 μM SOD. Error bars represent standard errors of the data obtained from duplicate experiments.

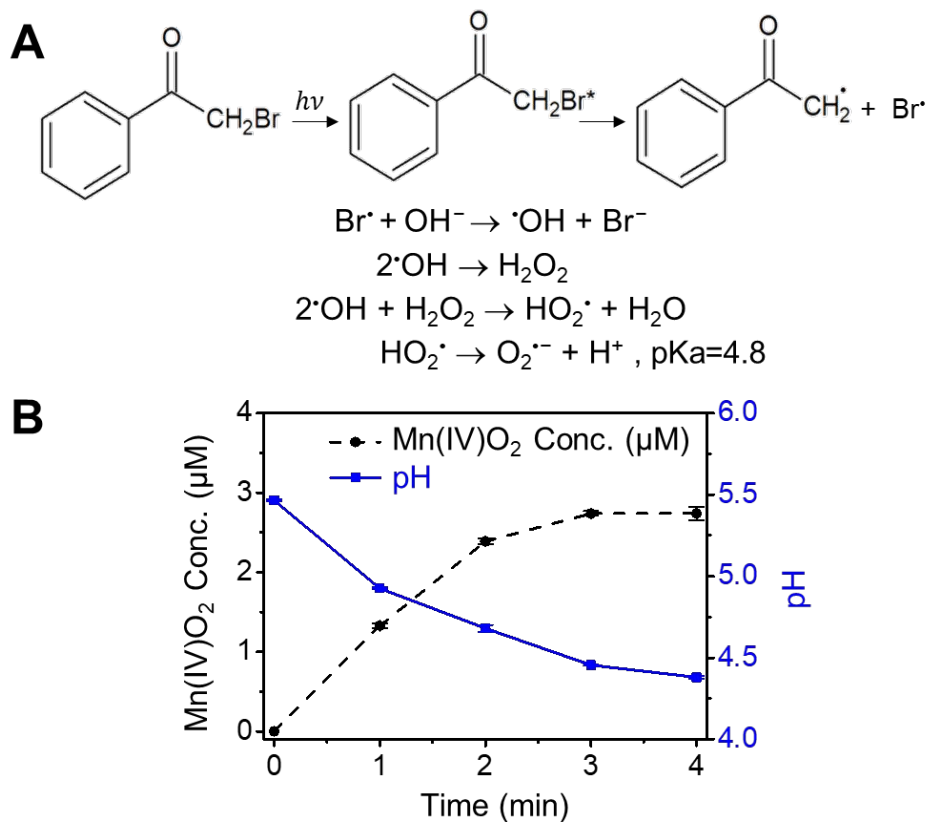


Figure 3. Mn oxidation by Br radicals generated from photolysis of bromoacetophenone (BrAP).

(A) Photolysis of BrAP can produce Br[•], which can react with OH⁻ to form •OH. O₂^{•-} is potentially formed in the sequential reactions. (B) Oxidized Mn concentration and pH value during photolysis of solution containing 0.1 mM MnCl₂, 1 mM BrAP, and 0.5 μM SOD. Error bars represent standard errors of the data obtained from duplicate experiments.

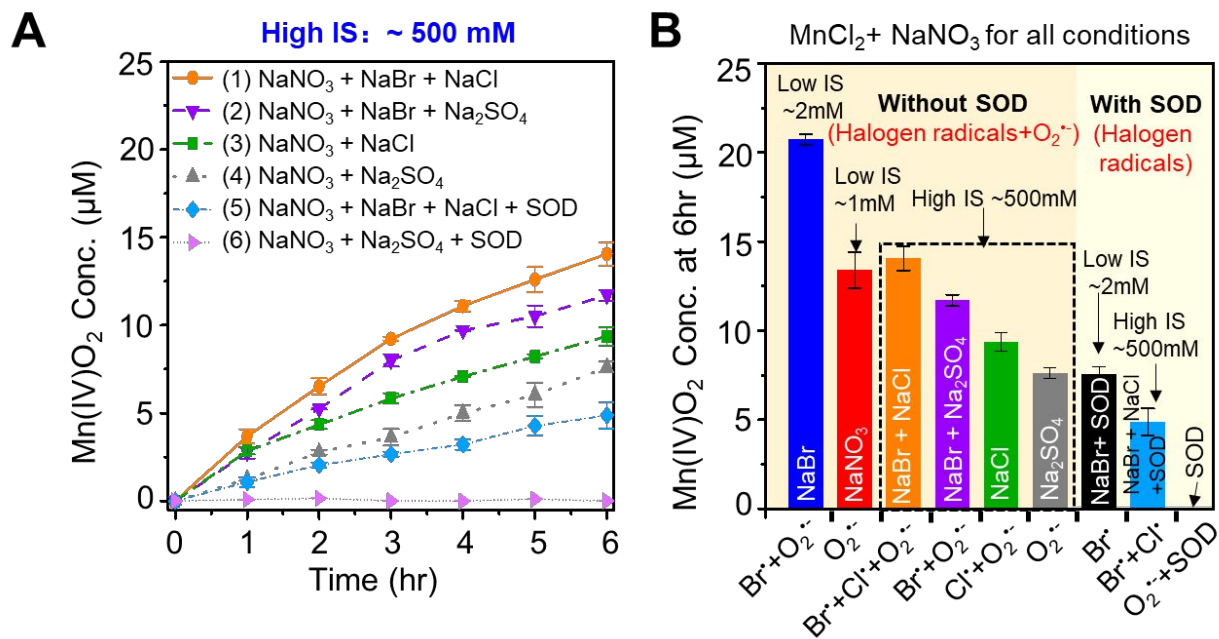


Figure 4. Comparison of the kinetics of Mn²⁺(aq) oxidation by O₂^{•-} or/and reactive halogen radicals (Br or/and Cl radicals). (A) Mn oxide generation over 6 hr of photolysis reaction of 0.1 mM MnCl₂, 1 mM NaNO₃ with different halide compositions at the same IS (~500 mM) without/with SOD. (1) 0.1 mM MnCl₂, 1 mM NaNO₃, 1 mM NaBr, and 500 mM NaCl; (2) 0.1 mM MnCl₂, 1 mM NaNO₃, 1 mM NaBr, and 166.7 mM Na₂SO₄; (3) 0.1 mM MnCl₂, 1 mM NaNO₃, and 500 mM NaCl; (4) 0.1 mM MnCl₂, 1 mM NaNO₃, and 166.7 mM Na₂SO₄; (5) 0.1 mM MnCl₂, 1 mM NaNO₃, 1 mM NaBr, 500 mM NaCl, and 0.5 μM SOD; and (6) 0.1 mM MnCl₂, 1 mM NaNO₃, 166.7 mM Na₂SO₄, and 0.5 μM SOD. (B) Summary of Mn²⁺ oxidation amounts of all conditions after 6 hr reaction. In the horizontal axis title, Br• stands for Br radicals (Br• and Br₂^{•-}), Cl• stands for Cl radicals (Cl• and Cl₂^{•-}), and Br• + Cl• stands for all Cl and Br radicals (Cl•, Br•, Cl₂^{•-}, Br₂^{•-}, and ClBr^{•-}).

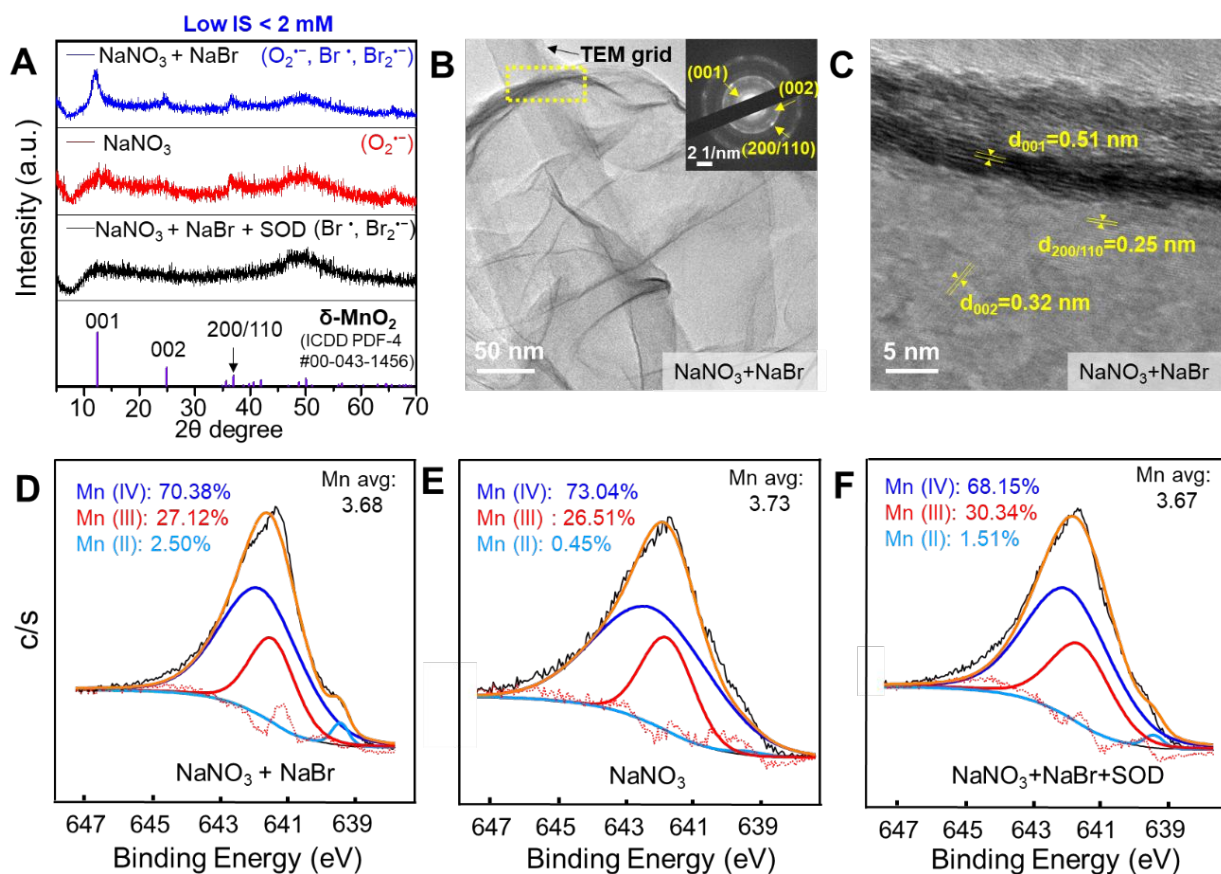


Figure 5. MnO₂ nanosheets formed by Br radicals. (A) δ -MnO₂ formation measured by HRXRD under the conditions of 0.1 mM MnCl₂, 1 mM NaNO₃, and 1 mM NaBr (blue); 0.1 mM MnCl₂ and 1 mM NaNO₃ (red); and 0.1 mM MnCl₂, 1 mM NaNO₃, 1 mM NaBr, and 0.5 μ M SOD (black) after 6 hr of reaction. (B and C) HRTEM images of the synthesized Mn oxide nanosheets under the condition of 0.1 mM MnCl₂, 1 mM NaNO₃, and 1 mM NaBr. The SAED patterns in (B) confirmed the formation of δ -MnO₂. (D-F) Average Mn oxidation states of the Mn 2p_{3/2} spectrum, calculated via Gaussian-Lorentzian fitting. Mn oxide solids were generated under the conditions listed in (A). At least duplicate tests were conducted for each condition. At least five different spots in the TEM grids were measured.

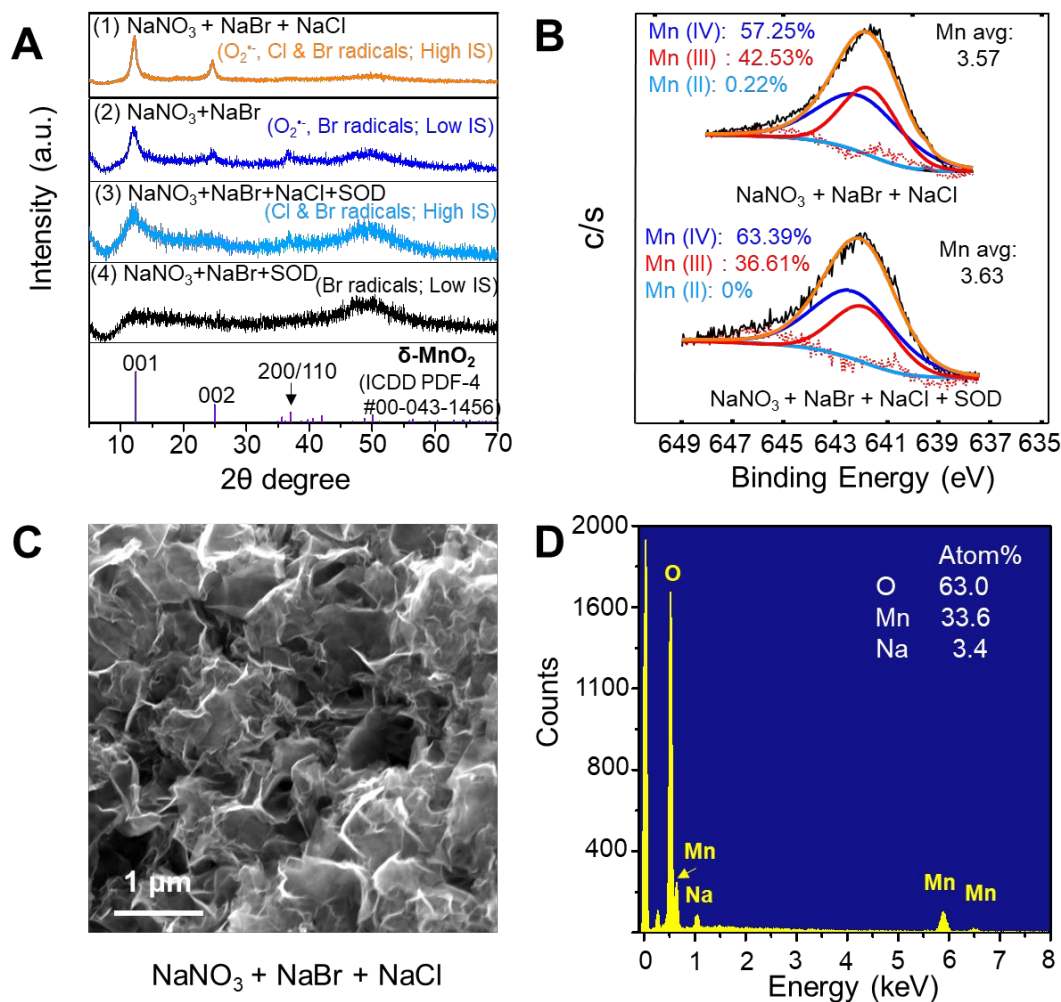


Figure 6. Comparison of $\text{O}_2^{\cdot-}$ or/and reactive halogen radicals on the characteristics of newly formed Mn oxide solids. (A) Comparison of HRXRD spectra of Mn oxide solids formed under the conditions of (1) 0.1 mM MnCl_2 , 1 mM NaNO_3 , 1 mM NaBr , and 500 mM NaCl ; (2) 0.1 mM MnCl_2 , 1 mM NaNO_3 , and 1 mM NaBr ; (3) 0.1 mM MnCl_2 , 1 mM NaNO_3 , 1 mM NaBr , 500 mM NaCl , and 0.5 μM SOD; and (4) 0.1 mM MnCl_2 , 1 mM NaNO_3 , 1 mM NaBr and 0.5 μM SOD. (B) Average Mn oxidation state of Mn $2p_{3/2}$ spectrum calculated via Gaussian-Lorentzian fitting. Mn oxide solids were formed under the conditions of (1) and (3). (C and D) Images showing surface morphology and elemental composition of Mn oxide formed under the condition of (1). At least duplicate tests were conducted for each condition. At least five different spots were measured for SEM imaging.